"An Analysis of a Prototype Permanent-Magnet Bearingless Motor using Finite Element Method"

by

Akira Chiba*1, Shigeru Onoya*1, Takeyoshi Kikuchi*1*
Masahide Ooshima*2, Satoru Miyazawa*2, Fukuzo Nakamura*1 and Tadashi Fuako*3

*1: Dept. of Electrical Eng.
Faculty of Sci. & Technology
Science University of Tokyo
2641 Yamazaki Noda Chiba
Japan 278
tel.+81(471)24-1501 Ext.3700
fax.+81(471)25-8651

*2:Dept. of Electr. Eng.
Science University of Tokyo
Suwa Junior College
5000-1 Toyohira, Chino
Nagano, Japan, 391-02
tel.+81(266)73-1201,
fax.+81(266)1231

*3: Dept. of Electrical and
Electronic Eng.
Tokyo Institute of Technology
2-12-1 Ookayama Meguro
Tokyo Japan 152
tel.+81(3)5734-2188
fax.+81(3)5734-2903

Abstract:An analysis is done for a prototype permanent magnet bearingless motor. A Finite Element Method program is employed to see the influence of demagnetization of permanent magnets. Several critical parts of rotor magnets are made clear for both torque and radial force generations. It is found that the most serious demagnetization occurs at the permanent magnet located at an edge of rotor poles. At this point, torque and radial force currents are the maximum. Moreover, it is shown that the serious condition occurs when the direction of the radial force flux is oriented so that negative mmf is imposed to the permanent magnet at the pole edge. The location of a critical permanent magnet and current conditions are made clear.

1. Introduction

Magnetic bearings have been employed in several applications such as machine tools, turbo-molecular pumps, compact generators, and flywheels. However, magnetic bearings still have problems in sizes and dimensions as well as costs.

Bearingless motors are high speed electric machines combined with magnetic bearing functions. The compactness of bearingless motors suggests the possibility of high power and high rotational speed drives. In addition, it is possible to simplify numbers of wirings and inverters required for magnetic levitation. It is also possible to reduce costs.

Developments of bearingless motors have been done in several countries [1-5]. Four-pole electric machines with additional two-pole radial force windings in its stator slots have been proposed with a simple controller [6-9]. Induction motors, synchronous reluctance motors and permanent magnet motors are demonstrated. Voltage and current at additional winding terminals have been found to be only several percents of motor volt-ampere requirements[8]. A decoupling control system configuration has been proposed for stable levitation under loaded conditions.

As for permanent magnet synchronous bearingless motors, a relationship between physical dimensions and performance has been made clear. Thin permanent magnets with small air-gap length are preferred to achieve high radial force for a current [9,10].

However, it is possible that demagnetization may occur if thin permanent magnets are employed. It is important to find the maximum radial force and torque of permanent magnet synchronous bearingless motors. It is very likely that there exist certain maximum values of radial force and torque, mainly determined by demagnetization of permanent magnets.

In this paper, an analysis is done for a prototype permanent magnet bearingless motor. A Finite Element Method program [11] is employed to see the influence of demagnetization of permanent magnets. Several critical parts of rotor magnets are made clear for both torque and radial force generations. It is found that the most serious demagnetization occurs at the permanent magnet located at one of the edges of rotor poles. In that condition, a torque current and a radial force current are the maximum. In addition, the direction of the radial force flux is oriented between rotor poles. The location of permanent magnet and conditions of the most serious demagnetization are made clear.

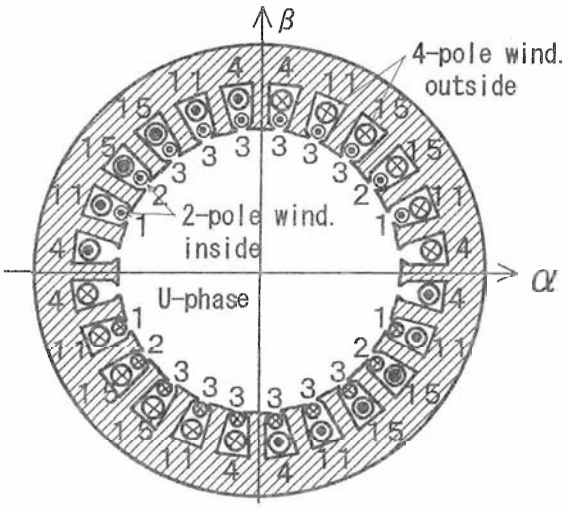

Fig.1 Winding distribution.

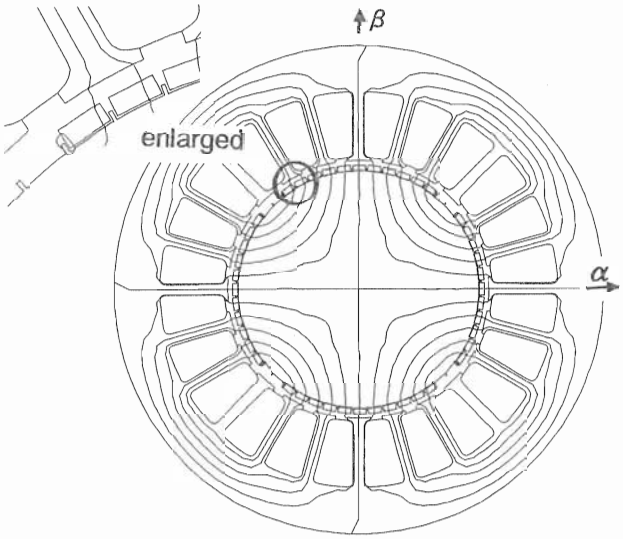

Fig.2 Flux distribution at no current.

2. Configuration of prototype machine

Fig.1 shows a stator iron core and winding configuration of a test machine. Both 4-pole windings and 2-pole windings are wound for torque and radial force generations, respectively. Three-phase symmetrical windings are wound for the two sets of windings. Only U-phase winding distribution is shown in Fig.1. The windings are arranged to generate sinusoidal distribution. The numbers indicate a number of series conductors in each slot. Two copper wires are connected in parallel. The diameters of each wire is 0.6mm. For

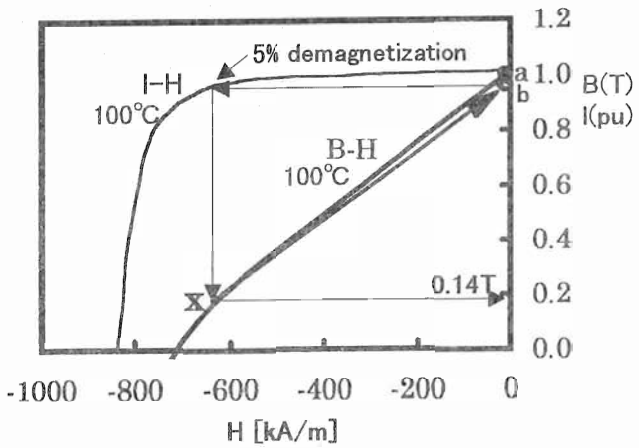

Fig.3 B-H and I-H curves.

the current density of 8A/mm², the rated line current is set to 6.4A. The outer and inner diameters of stator iron core is 95mm and 50mm, respectively. The stack length of the iron core is 50mm. The iron core is made of laminated silicon steels.

Fig.2 shows the rotor structure and flux distribution at no load. Permanent magnets having thickness of 1mm are pasted on the surface of rotor iron. Small projections of silicon steel are fabricated to paste permanent magnets easily. The outer diameter of silicon steel neglecting the small projections is 46mm. Thus, the air-gap length between the stator inner surface and outer surface of permanent magnets is 1mm. SmCo permanent magnets (REC26, TDK) are employed in the test machine. The permanent magnets are pasted to produce four-pole flux distribution. Permanent magnets are not pasted at the edge of rotor poles to generate smooth sinusoidal flux distribution.

In Fig.2, the rotor is positioned at the center of the stator. No currents are supplied to the stator windings. Symmetrical four-pole fluxes are generated by permanent magnets.

Fig.3 shows B-H and I-H curves of SmCo magnets used in prototype bearingless motor. These curves have variations depending on the temperature. The characteristics become worse as temperature increases. In order to consider the worst case, the temperature of 100C is assumed in this paper. If a permanent magnet is magnetically shorted, the operating point is the point a as indicated. From I-H curve, 5% of demagnetization occurs at H= - 640kA/m. The indicated point x shows the flux density at this point, i.e., 0.14T.

Once a permanent magnet is reached to the point x, then, 5% demagnetization occurs. Even though the permanent magnet is magnetically shorted, the operating point does not return to the point a, but it moves to the point b. The decrease of

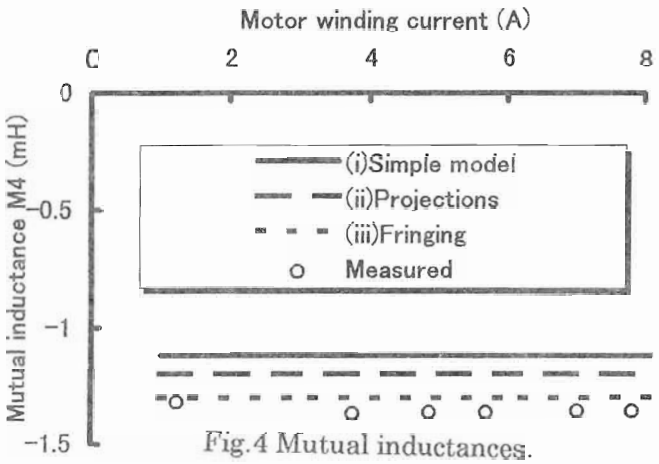

Fig.4 Mutual inductances.

5% can be seen compared with the point a. It is possible to determine that this point is a limitation of demagnetization. This limitation of demagnetization may seem to be a rather severe condition for practical applications.

3. Verification of FEM model

It is important to verify a FEM model of a prototype test machine. In the case of permanent magnet type bearingless motors, there are several particular points to be considered. These are summarized as follows;

(i)Small projections at the surface of a rotor iron core.

(ii) Fringing fluxes at coil ends.

(iii) Small non-magnetic space between permanent magnets and a rotor iron core. This space is filled by adhesive materials in a test machine.

Fig.4 shows a mutual inductance M_4 between 4-pole windings. The value of the mutual inductance is negative because three-phase windings are wound. This mutual inductance is chosen because measurements of this inductance is precise and easy in experiments. The measured mutual inductances are plotted as a function of exciting current. The mutual inductance is almost constant because the air-gap length is wide in permanent magnet machines.

Three calculated curves are also plotted for comparisons. These curves are drawn based on a model constructed as follows;

(i) Simple model: the rotor iron is assumed as smooth circle.

(ii) Small projections on rotor surface are considered.

(iii) Small projections and fringing flux at coil ends are included.

It is seen that errors are reduced as the FEM model is improved. There are about 7% errors

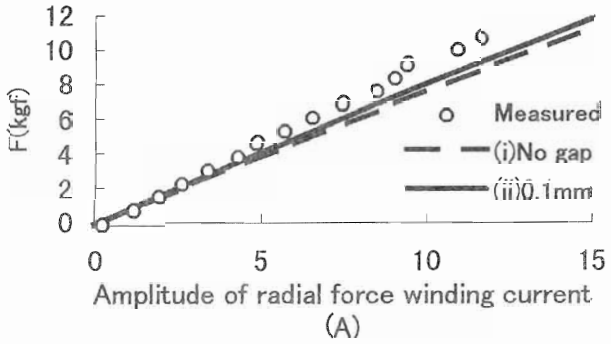

Fig.5 Radial force and current.

neglecting small projections. In addition, additional 9% errors are generated neglecting fringing fluxes at coil ends. In FEM analysis, it is rather difficult to construct small projections because of the limitation of element numbers. However, these projections are found to be included in FEM model. These are included in the following analysis.

Fig.5 shows the relationship between radial force and radial force winding current. Radial forces are applied to the test machine and amplitudes of radial force winding currents are measured. These measured values are plotted.

Two theoretical curves are also drawn as results of FEM analysis. These results are based on the following FEM models.

(i) Permanent magnets are placed on the rotor iron surface without air-gap.

(ii) The air-gap length between rotor iron and permanent magnets is considered to be 0.1mm. This air-gap length represents non-magnetic adhesive material in the test machine.

In the case of (i), significant short circuit flux paths are generated through permanent magnet, small projections and rotor irons. It is seen that the case (ii) is closer to the measured points. The calculated values are still less than the measured values. These errors are caused by the difference in temperatures. The FEM analysis is done at 100C, however, experiments are done around 20C.

4. Demagnetization caused by torque current

Fig.6 shows the flux distribution at 2.3 times of the rated torque current. The symmetrical three phase currents are supplied to the stator windings. It can be seen that the 4-pole flux distribution is rotated in clockwise direction. The rotor is producing torque in clockwise direction, too. The most serious demagnetization occurs at the four parts of the rotor as indicated by circles. These permanent magnets are located at the edge of rotor

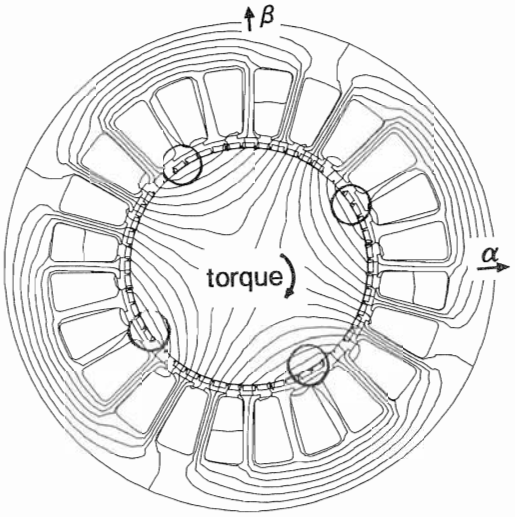

Fig.6 Flux distribution at load.

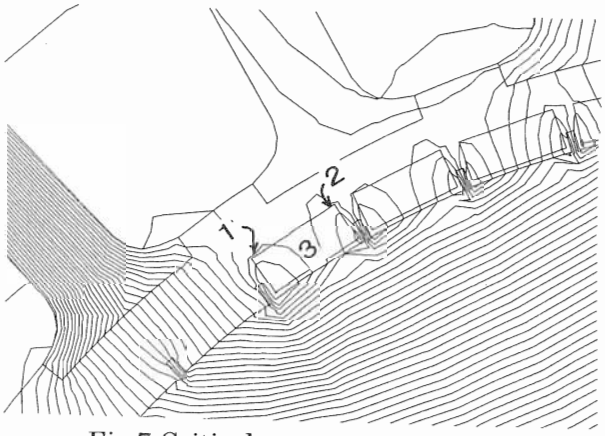

Fig.7 Critical permanent magnet.

magnetic poles.

Fig.7 shows an enlarged flux distribution at the edge of rotor poles. It is seen that the most flux, generated in the permanent magnet located at the edge of the rotor pole, return to the permanent magnet through the small projections. No flux goes through stator teeth. Thus, flux density at the air-gap above the permanent magnet is very low, less than 0.1T. As a result, the flux density inside of the permanent magnet is also decreased. The minimum flux density can be seen at the edges of the permanent magnet as indicated 1 and 2. The flux density at the point indicated 3, i.e., the center of permanent magnet, is slightly higher than those at the points 1 and 2.

Two criteria of demagnetization can be determined based on the flux density in a permanent magnet located at the edge of the rotor poles as the followings;

(i) The flux density, oriented to the direction of pre-magnetization, at the edges of permanent magnets are decreased to 0.14T.

(ii) The flux density at the center of the permanent magnet is decreased to 0.14T.

The flux density of 0.14T is corresponding to 5% demagnetization as shown in Fig.3. In the case of (i), only small area at the edges of permanent magnets is demagnetized by 5%. Thus, the most parts of permanent magnets are not demagnetized. The demagnetization is very slightly. In the case of (ii), a half part of the critical permanent magnets are demagnetized by 5%. It is also unavoidable that some parts of permanent magnets are demagnetized less than 0.14T. The residual flux density of this permanent magnet may decrease more than 5%.

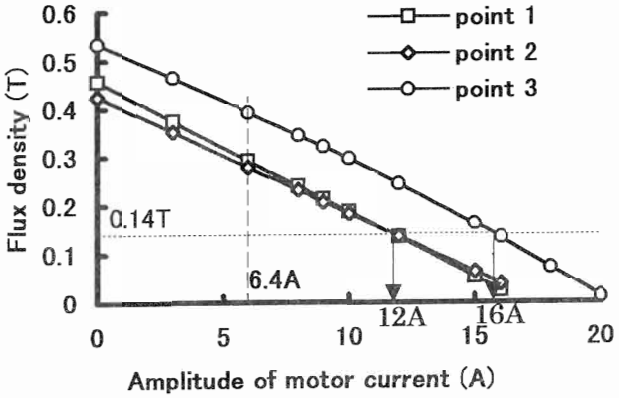

Fig.8 Flux densities in permanent magnet.

Fig.8 shows the flux densities of three points of a critical permanent magnet in pre-magnetized direction. These points 1 to 3 are corresponding to the points indicated as 1 to 3 in Fig.7. The horizontal axis is torque current. It can be seen that the flux densities are proportionally decreased as the torque current is increased. The flux densities are more than 0.14T at the rated torque current of 6.4A. Thus, there is no demagnetization. The flux density of 0.14T is reached at 12A for case (i) and 16A for case (ii).

Torque is also calculated. It is noted that torque is generated almost proportional to the torque current up to 16A. A decrease in torque is seen over 16A. This decrease is resulted from demagnetization.

5. Demagnetization by radial force current

Fig.9 shows flux distribution with radial force winding current of 12A, i.e., almost twice of the rated current. The 4-pole symmetrical flux distribution, generated by permanent magnets as shown in Fig.2, is unbalanced by 2-pole fluxes. The 2-pole fluxes are oriented to the β-axis direction. Flux densities at the upper air-gap are increased,

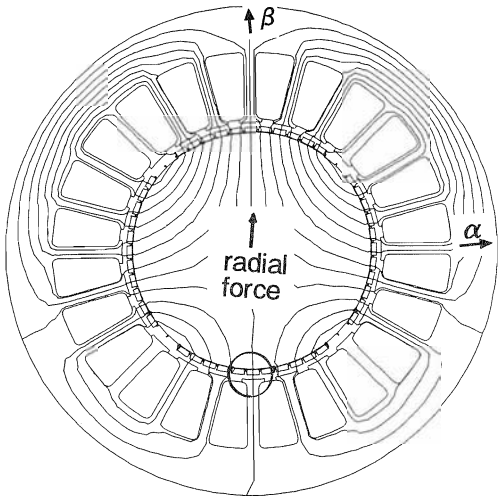

Fig.9 Flux distribution with radial force.

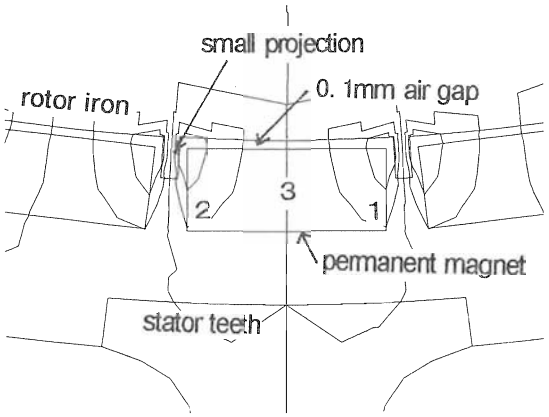

Fig.10 Critical permanent magnet.

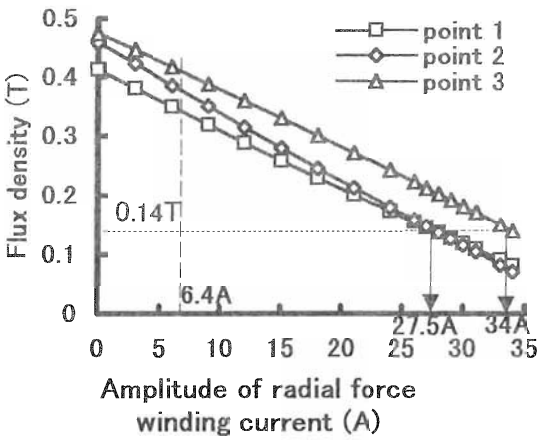

Fig.11 Flux densities in permanent magnet.

but these are decreased in the air-gap under the rotor. Radial force is generated in β -axis direction. In this flux distribution, the most serious demagnetization occurs in the permanent magnet located at the bottom of the rotor as indicated by a circle.

Fig.10 shows an enlarged flux distribution around the critical permanent magnet. Flux plots are not smooth enough because of element limitation of 10,000. However, basic phenomenon can be seen. Most of the fluxes come out from permanent magnet and go through small projections and a rotor iron. Flux densities at points 1 and 2, located at the edge of permanent magnets, are decreased. The point 3 indicated the center of the critical permanent magnet.

Fig.11 shows the flux densities at points 1 through 3 as a function of radial force winding current. The flux densities of these points are above 0.14T at the rated current of 6.4A. Demagnetization is avoided. Radial force is 5kgf. The maximum radial force winding current can be increased up to 34A, which corresponds to 21kgf.

6. Torque and radial force currents

In section 4, the critical permanent magnet is found to be located at four edges of rotor poles. Fig.12(a) shows flux directions Ψ_p of permanent magnets. The direction of armature reaction fluxes Ψ_t, which are generated by torque currents are also shown. The critical permanent magnets are located at the area indicated by A-D.

In section 5, it is shown that a critical permanent magnet is only one, which direction of pre-magnetization is against radial force flux. Thus, a permanent magnet at the area D face severe condition if radial force fluxes Ψ_2 are oriented as shown in Fig.12(a).

Fig.12 (b) shows the flux distribution at 1.5 times of rated current in both motor and radial force windings. The most critical permanent magnet is indicated by a circle. In this flux distribution, a radial force is generated in the direction of F as shown in Fig.12(b).

Fig.13 shows flux densities of the critical permanent magnet as a function of both radial force and motor windings. Both windings carry the same amount of three-phase current. Flux densities at two edges, i.e., points 1 and 2, as well as center point 3 of permanent magnets are shown. It is seen that flux densities are above 0.14T at the rated current of 6.4A for both radial force and motor windings. Partial demagnetization may occur at 1.5 times of rated current because the flux densities at the edges of permanent magnets are below 0.14T. At a current of 11.2A, the flux density at the center of critical permanent magnet becomes 0.14T. The radial force and torque are 9kgf and 7.7Nm, respectively.

7. Conclusion

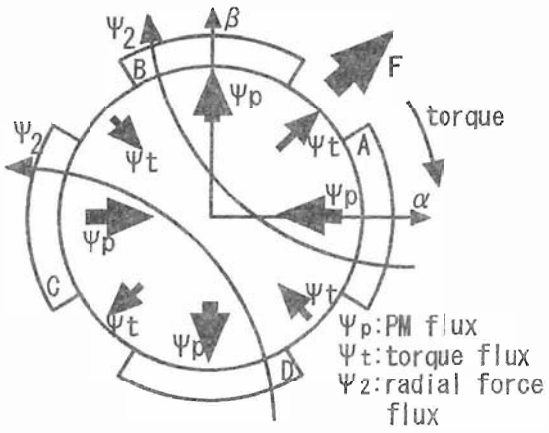

(a) PM, torque and radial force fluxes.

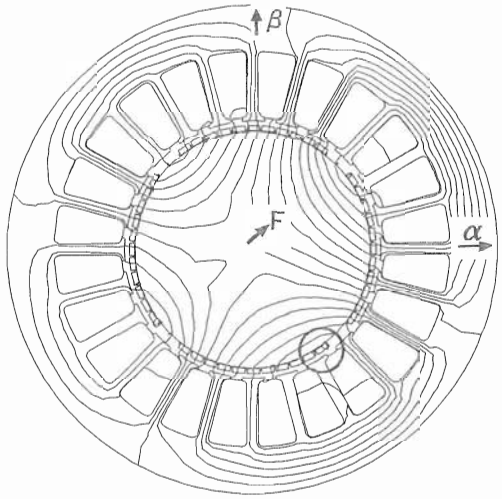

(b) The most critical flux distribution.

Fig.12 Flux orientation and demagnetization.

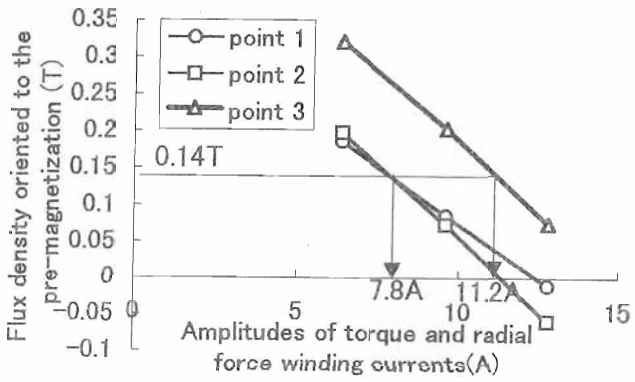

Fig.13 Flux densities in permanent magnet.

In this paper, FEM analysis is done to see the limitation of demagnetization of permanent magnets in a prototype bearingless motor. It is found that the most serious demagnetization occurs at a permanent magnet located at an edge of rotor poles. The radial force flux is oriented opposite to the pre-magnetized direction of that permanent magnet.

A test machine is found to be free from demagnetization, up to 1.7 times of the rated current for both radial force and motor windings.

References

[1]Bosch, R., "Development of a Bearingless Electric Motor", Proc. of ICEM'88 vol.3 pp.373-375

[2]A.Ortiz Salazar, W.Dunford, R.Stephan, E.Watanabe, "A Magnetic Bearingl System using Capacitive Sensors for Position Measurement", IEEE Trans. on Magnetics vol.26 no.5 1990 pp.2541-2543

[3]R.Schob "Applications of Lateral-Force-Motor (LFM)", Proc. of Int'l Power Electronics Conf., IPEC'95-Yokohama pp.358-363

[4]T.Ohishi, Y.Okada and K.Dejima, "Analysis and Design of a Concentrated Wound Stator for Synchronous Type Levitated Motor", Proc. of 4th Int'l Symp. on Magnetic Bearings, pp.201-206, 1994

[5]"A Radial Active Magnetic Bearing Having a Rotation Drive", Patent Specification 1 500 809, 1978

[6]Akira Chiba, Kouji Chida and Tadashi Fukao," Principle and Characteristics of a Reluctance Motor with Windings of Magnetic Bearing", Proc. of Int'l Power Electronics Conf., IPEC'90-Tokyo, pp.919-926

[7]O.Ichikawa, C.Michioka, A.Chiba and T.Fukao,"A Decoupling Control Method of Radial Rotor Positions in Synchronous Reluctance Type Bearingless Motors", Proc. of Int'l Power Electronics Conf., IPEC'95-Tokyo vol.1 pp.346-351

[8] Yasuhisa Takamoto, Akira Chiba and Tadashi Fukao,"Test Results on a Prototype Bearinless Induction Motor with Five-Axis Magnetic Suspension", Proceedings of 1995 International Power Electronics Conference (IPEC-Yokohama'95) vol.1, pp.334-339, April 7, 1995

[9] Masahide Ooshima, Satoru Miyazawa, Tazumi Deido, Akira Chiba, Fukuzo Nakamura and Tadashi Fukao, "Characteristics of a Permanent Magnet Type Bearingless Motor", IEEE Transaction on IA, vol.32, no.2, pp.363-370, 1996 March/April

[10] Masahide Ooshima, Akira Chiba, Tadashi Fukao and M.Azizur Rahman, "Design and Analysis of Permanent Magnet-Type Bearingless Motors", IEEE Trans., Indus. Electr., vol.IE-43, no.2, pp.292-299, 1996

[11] PC=Opera Manual, Vector Fields Co. 1996.